

Controlling quantum vortex dynamics and vortex-antivortex annihilation in Bose-Einstein condensates with optical lattices

Francesco Ancilotto ^{1,2} and Luciano Reatto ³

¹*Dipartimento di Fisica e Astronomia “Galileo Galilei” and CNISM, Università di Padova, via Marzolo 8, 35122 Padova, Italy*

²*CNR-IOM Democritos, via Bonomea, 265 - 34136 Trieste, Italy*

³*Dipartimento di Fisica, Università degli Studi di Milano, via Celoria 16, 20133 Milano, Italy*



(Received 21 April 2024; accepted 14 June 2024; published 3 July 2024)

Superfluids with strong spatial modulation can be experimentally produced in the area of cold atoms under the influence of optical lattices. Here we address ^{87}Rb bosons at $T = 0$ K in a flat geometry under the influence of a periodic potential with the Gross-Pitaevskii theory. The statics and dynamics of vortex excitations are studied in the case of one-dimensional (1D) and of two-dimensional (2D) optical lattices, as function of the intensity of the optical lattice. We compute how the vortex energy depends on the position of its core and the energy barrier that a vortex has to surmount in order to move in the superfluid. The dynamics of a vortex dipole, a pair of vortices of opposite chirality, differ profoundly from the case of a uniform superfluid. In the 1D case, when parallel ridges of density are present, the dynamics depends on the positions of the two vortices. If they are in the same channel between two ridges, then the two vortices approach each other until they annihilate each other in a short time. If the two vortices are in distinct channels, the dipole undergoes a rigid translation but with a velocity depending on the intensity of the optical lattice and this translation velocity can even change sign with respect to the case of the uniform superfluid. Superimposed on this translation an oscillatory motion is also present. A superposition of translation along a channel and an oscillation is also found with a single vortex when the system is bounded inside a circular trap. These oscillatory motions can be both longitudinal, i.e., along the channel, as well as transverse. In all cases the transverse motions are one sided, in the sense that the vortex core never crosses the equilibrium position nearest the starting position. In the case of the 2D lattices we study (square, triangular, and honeycomb), the two vortices of a dipole move mainly by jumps between equilibrium positions and approach each other until annihilation. This behavior has some similarity with what has been found for a vortex dipole in the supersolid state of dipolar bosons. We show that a rapid ramp down of the optical potential improves the visibility of the density holes at the vortex core.

DOI: [10.1103/PhysRevA.110.013302](https://doi.org/10.1103/PhysRevA.110.013302)

I. INTRODUCTION AND SUMMARY

One of the key properties of a superfluid is the presence of quantized vorticity. In the case of bosons this has been experimentally verified in superfluid ^4He [1] and in Bose-Einstein condensates (BEC) of cold atoms [2]. A quantum vortex is an excitation of the system with quantized circulation and angular momentum and usually such excitation is studied in a superfluid that is uniform or with an inhomogeneity that is weak on the scale of the healing length of the superfluid. At present there is the possibility of studying vortices in spatially strongly inhomogeneous systems, both in terms of the spatial scale as well as in terms of large contrast between the maximum and the minimum densities. In the realm of cold atoms it is possible to generate a periodic potential (optical lattice, OL) acting on the atoms and this potential is obtained by standing waves of suitable crossing light beams [3]. The period of the optical lattice can be comparable to the healing length and the local density can vary even by orders of magnitude. A recent experiment [4] has verified the theoretical prediction [5] that even at the lowest temperatures the superfluid fraction of the superfluid is less than unity due to the induced density modulation.

Another system that is predicted to be a spatially strongly inhomogeneous superfluid is a submonolayer of ^4He adsorbed on a substrate of fluorographene, a sheet of graphene decorated by fluorine atoms. The adsorption potential of a He atom on this substrate is strongly corrugated but not so much to cause localization of the atoms like on graphite. Theory [6] shows that the system is superfluid and the local density has a very large excursion in space. A supersolid (SS) offers another example of a strongly inhomogeneous superfluid. In a SS the inhomogeneity arises from a spontaneous broken symmetry of the translational invariance. Such SS state has been found in cold-atom systems, for instance, in dipolar bosons like ^{164}Dy [7]. Again the local density can vary by a large amount and the healing length is comparable with the lattice parameter of the SS.

Different ways have been devised to create vortices in BEC superfluids, such as phase imprinting [8], by dragging obstacles [9], by means of artificial gauge fields [10], and more recently using a versatile, deterministic two-dimensional (2D) vortex collider in homogeneous atomic superfluids [11].

Complex dynamics of vortices under the action of the optical lattice in a trapped BEC sample have been unveiled in a theoretical study of vortices within the two-dimensional

Gross-Pitaevskii (GP) equation with the OL and magnetic trap [12], where it was found that depending on the phase of the OL relative to the parabolic magnetic trap, it is possible either to trap the vortex at the center of the trap, or the vortex moves along an unwinding spiral, towards the periphery of the trap.

The interplay of lattice physics and rotation physics was studied by calculating the vortex-lattice structures near a Mott transition [13]. A single BEC loaded in a rotating OL can show a rich variety of vortex structural transitions [14].

There have been predictions of novel types of vortex states of repulsive BECs confined by a shallow optical lattice (matter-wave gap vortices), which are spatially localized and dynamically stable in 2D as well as in three-dimensional (3D) optical lattices [15].

A somewhat related topic (vortex solitons in BEC stabilized by optical lattices) has been addressed in Ref. [16].

Interestingly, vortex dynamics in nonhomogeneous systems can be linked to “glitches” in rotating pulsars, i.e., a sudden speedup of the spinning stars, occurring at random intervals. These events are believed to be a manifestation of the presence of a superfluid component in the stellar interior, the glitch occurring when many vortices jump from the inside of the star to the solid crust, transferring angular momentum and thus speeding it up. It has been shown recently, using cold-atom experiments as analogs of neutron stars, that this requires simultaneous crystalline and superfluid phases, i.e., a supersolid state [17].

A subject that apparently has received very little attention is the behavior of vortex dipoles. Such configurations have been experimentally obtained in BEC in the work of Ref. [9]. However, topics such as the interaction of such dipoles and the ensuing dynamics are still unexplored. Our study provides an insight into these issues, and how they are modified by optical lattice.

All this gives a motivation for studying vortices in strongly inhomogeneous superfluids, the aim of this paper. We show how strongly the dynamics of vortices and the lifetimes of pairs of vortex-antivortex are affected by an optical potential. The experimental realization of generation of vortex dipoles in a suitable trap for cold atoms [11] opens the possibility of experimental verification of our predictions.

Vortices in the SS state of matter in dipolar bosons have been addressed [18–21] in recent years and some relevant phenomena have been uncovered, like a reduced angular momentum associated to the quantum of circulation [18]. A peculiar behavior has been found [21] in the dynamic of a vortex dipole, i.e., a pair of vortices of opposite chirality, in a SS. In a uniform superfluid, when the distance l between the two vortices is larger than the healing length ξ , the pair is a stable entity and moves with a constant velocity as a rigid body in a direction perpendicular to the vector \vec{l} joining the two vortices. Contrary to this, in dipolar bosons in a SS state it was found that the two vortices move by jumps between equilibrium sites in the lattice and approach each other until the two vortices annihilate themselves in a short time. At the basis of this behavior is a basic property of a vortex in a SS: it is energetically favorable to have its core at a discrete set of positions, the locus of minimum density. The natural question is if such properties are specific of a SS state or if they are generic ones when a density modulation is present, whatever

is its origin. To answer this question we address in this paper the study of bosons in an external periodic potential like that produced by light standing waves. We study the ground state and vortices of the standard model of BEC, pointlike bosons with a contact interaction, in the case of ^{87}Rb with the Gross-Pitaevskii equation in an external periodic potential $V_{\text{ext}}(\vec{r})$. We consider the case of modulation in one dimension (1D) and in two dimensions (2D) for three lattices: square, triangular, and honeycomb.

The system is subject to periodic boundary conditions in all three space directions, and translational invariance along the z direction perpendicular to the lattice potential plane is assumed. The length in the z direction is of order of the healing length of the superfluid so that the system can be considered as a quasi-two-dimensional system.

In the studied range of intensity of our optical potentials we find that the bosons are in a superfluid state with a reduced superfluid fraction. The local density is a periodic function of position reflecting the symmetry of the optical potential and the excursion between maxima and minima can be very large, depending on the strength of the modulation of $V_{\text{ext}}(\vec{r})$. In a uniform superfluid the vortex excitation energy ΔE_v does not depend on the position of its core. On the contrary, in the presence of the optical potential ΔE_v depends on the position of its core and it is a strong function of the local density. The minima of ΔE_v are at the positions of the minima of the local density, i.e., at the maxima of $V_{\text{ext}}(\vec{r})$, consistently with the observation of pinning of the vortex at the low-density site of an OL was observed [22]. Therefore, ΔE_v is a periodic function of position and this has a dramatic effect on the dynamics of vortices. The flow field of a vortex is strongly deformed from the circular shape of the uniform case and we characterize the vortex excitation energy and its structure as function of the amplitude of the optical potential.

The dynamics of a vortex dipole is also strongly affected by the presence of the optical potential. For a 2D potential, where the equilibrium positions of the vortex are isolated points, the dipole moves mainly by jumps between equilibrium sites approaching each other until the two vortices annihilate themselves in a short time. In our theory no thermal or stochastic effects are present and these jumps are manifestations of tunneling of the vortices between equilibrium sites.

The behavior is different in the case of a 1D modulation where the equilibrium positions for a vortex form a series of parallel lines in the $x - y$ plane.

If the two vortices of the dipole are located in the same channel they do not translate but they move one against the other until they annihilate and the excitation energy goes into phonons of the superfluid. If the two vortices are located in adjacent channels they move along these channels and the motion is a composition of a uniform translation and of an oscillation. In all cases the translation velocity of the pair differs from that expected for a uniform superfluid and it can even invert the direction of motion for large amplitude of the optical potential. A combination of translation and oscillation is found also for a single vortex in a trap in presence of a 1D OL. The frequency of this oscillation is the same as in the case of a vortex dipole moving along two neighboring channels. Therefore, this oscillatory motion seems to be an intrinsic and unique character of the motion of a vortex moving along a

channel. Notice that this oscillatory motion is quite different from that of a massive particle around a minimum energy position because the vortex oscillation is one sided, i.e., the vortex never crosses the position of the minimum energy and it remains on the side from which it started.

The local density goes to zero at the position of the vortex core. In the case of a strong modulation experimentally it can be difficult to detect the presence of a vortex because there is a small contrast between the vanishing density of the vortex core and the small value of the density at the minima of the modulated system. We show that by starting from a state with a number of vortices in the modulated superfluid, such vortices remain in the homogeneous superfluid after that the optical potential is suddenly removed, allowing for an easier visual detection due to the increased contrast between the vanishing density at the core positions and the density of the surrounding, almost homogeneous, phase.

The content of the paper is as follows. In Sec. II the theory and the computational method are described. In Sec. III the ground state, the vortex state, and the dynamics of a vortex pair are studied in the case of 1D optical potential. In this section we study also the dynamics of a vortex when the system is confined in a circular trap in the $x - y$ plane. The case of 2D optical potentials is studied similarly in Sec. IV. In Sec. V we study the time evolution of a confined system after the optical potential is removed, as a way to directly image vortex positions in these highly inhomogeneous systems. Our conclusions are contained in Sec. VI.

II. METHOD

The Gross-Pitaevskii (GP) energy functional for the Bose system reads as

$$E = \int d\mathbf{r} \left[\frac{\hbar^2}{2m} |\nabla\psi(\mathbf{r})|^2 + V(\mathbf{r})\rho(\mathbf{r}) \right] + \frac{1}{2}g \int d\mathbf{r} \rho^2(\mathbf{r}), \quad (1)$$

where $V(\mathbf{r})$ and $\rho(\mathbf{r}) = |\psi(\mathbf{r})|^2$ represent the external potential and the boson number density, respectively. The coupling constant is $g = 4\pi a_s \hbar^2/m$, m being the atomic mass. The number density ρ is normalized such that $\int_V \rho(\mathbf{r}) d\mathbf{r} = N$ where N is the total number of atoms. As model system we take ^{87}Rb atoms and the scattering length a_s describing the (repulsive) Rb-Rb interaction is $a_s = 100.4 a_0$ [23] (a_0 being the Bohr's radius).

Minimization of the action associated to Eq. (1) leads to the following Euler-Lagrange equation (GP equations):

$$i\hbar \frac{\partial\psi(\vec{r}, t)}{\partial t} = \left[-\frac{\hbar^2}{2m} \nabla^2 + V(\vec{r}) + g\rho(\vec{r}, t) \right] \psi(\vec{r}, t) \\ \equiv H\psi(\vec{r}, t). \quad (2)$$

When steady states are studied, the left-hand side of Eq. (2) is replaced by $\mu\psi(\vec{r}, t)$ where μ is the chemical potential. The numerical solutions of Eq. (2) provide the time evolution of the ^{87}Rb system with arbitrary N in three dimensions. The same equation in imaginary time allows us to obtain stationary-state solutions starting from a suitable initial function. μ is determined so that the desired value of N is achieved. We consider an external potential depending only in x and y .

In our computations the length L_z of the computation box is much smaller than the other sides. Under this condition we simplify the computation by neglecting the dependence of ψ on the z coordinate and therefore the calculations become effectively two dimensional. Accordingly, vortex states considered here are not subject to three-dimensional instabilities like corrugation or bending of the vortex core as the transverse dimension is effectively suppressed. For this reason often in the following we will describe the properties of the system as it appears in the $x - y$ plane only.

Equation (2) is solved either in real or imaginary time by using Hamming's predictor-modifier-corrector method initiated by a fourth-order Runge-Kutta-Gill algorithm [24]. The spatial mesh spacing and time step are chosen such that, during the real-time evolution, excellent conservation of the total energy of the system is guaranteed.

We will use in this work different forms for the external potential V appearing in the GP equation (2). In particular, we will consider *periodic* potentials both in one dimension and in two dimensions, as described in the following sections. These potentials are easily produced in experiments using crossed laser fields with appropriate wavelengths (optical lattices, OL).

III. ^{87}Rb IN 1D OPTICAL LATTICE

One-dimensional lattice potentials are often used in experiments. In the simplest form, like the one used here, they produce modulated density patterns characterized by a periodic alternation of stripes of maxima and minima in the gas density. Here we consider the form

$$V_{\text{OL}}(x) = 2V_0 \cos^2(kx). \quad (3)$$

The wave vector k determines the lattice constant of the periodic potential $d = 2\pi/k$. For the cases investigated here we chose $d = 60\,000 a_0 = 3.175 \mu\text{m}$. The sizes of the supercell in the $x - y$ plane are, for most of the calculations done, $L_x = L_y = 44.45 \mu\text{m}$, corresponding to 14 stripes in the x direction, although for the sake of visibility the plots shown in this paper are often limited to smaller portions of the supercell.

Along the z direction we chose the value $L_z = 1.429 \mu\text{m}$. The total number of atoms N in most of our calculations is chosen so that it corresponds to an areal density $n_a = N/(L_x L_y) = 9.92 \mu\text{m}^{-2}$. In the following, some calculations will be performed using larger supercell sizes L_x, L_y , corresponding to 20 stripes in the x direction. However, we will always take the number of atoms N such that the areal density $n_a = N/(L_x L_y)$ is not changed.

The healing length for the uniform system ($V_0 = 0$) is $\xi = \hbar/\sqrt{2m\mu} = 1.039 \mu\text{m}$, where $\mu = g\rho$ is the Rb chemical potential in the absence of the lattice modulation. Notice that L_z is of the same order of magnitude of the healing length, and therefore our system can be considered quasi-2D. Due to the imposed translational invariance along the z direction, along which the density is therefore constant, the calculations are effectively two dimensional, involving a spatial discrete mesh only in the $x - y$ plane.

We will consider different values for the potential strength V_0 in the following, and often the following values $V_0 = 2, 4, 7, 9 \times 10^{-14}$ Ha have been used.

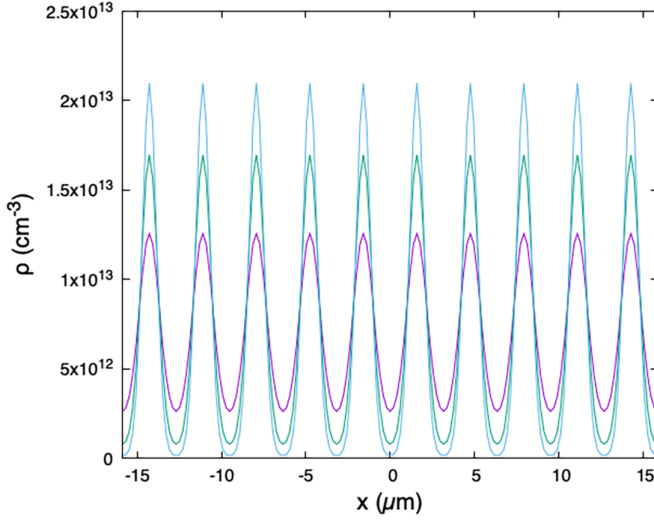


FIG. 1. Density profiles (in units of cm^{-3}) along the x axis, for different values of \tilde{V} . From the highest to the lowest peak values: $\tilde{V} = (7, 4, 2)$.

It is customary to express the lattice well depths V_0 in terms of the so-called recoil energy as $V_0 = sE_R$, where

$$E_R = \frac{\hbar^2 \pi^2}{2md^2}. \quad (4)$$

In the present case $E_R = 8.600 \times 10^{-15}$ Ha. The values of V_0 quoted above therefore correspond to $s = 2.3, 4.6, 8.1, 10.5$. For much larger values of the s bosons are expected to become localized forming rows of independent quasi-one-dimensional superfluids.

In the following we will use a more manageable notation where the optical potential strength V_0 is expressed in terms of an adimensional quantity \tilde{V} such that $V_0 = \tilde{V} \times 10^{-14}$ Ha $= \tilde{V} \times 3.158$ nK.

In Fig. 1 we show for some values of \tilde{V} the density along the x axis, the direction of the modulation showing the periodic alternation of minima and maxima in the density profile. The values of the density at these extrema are reported in Table I, together with the calculated chemical potentials.

It can be noticed that already an intensity $\tilde{V} = 4$ the maximum density is 10 times larger of the minimum density. Despite such large inhomogeneity the system is superfluid. The superfluid fraction can be computed from the nonclassical

TABLE I. \tilde{V} is the amplitude of the periodic potential; ρ_{\min} and ρ_{\max} are the density values at the bottom and top of the modulated density; μ is the chemical potential and f_s is the superfluid fraction in the x direction computed from the nonclassical translational inertia.

\tilde{V}	$\rho_{\min} (\text{cm}^{-3})$	$\rho_{\max} (\text{cm}^{-3})$	μ (nK)	f_s
0	6.943×10^{12}	6.943×10^{12}	2.584	1
2	2.609×10^{12}	1.256×10^{13}	8.062	0.744
4	0.777×10^{12}	1.696×10^{13}	11.923	0.355
7	0.136×10^{12}	2.098×10^{13}	15.839	0.095

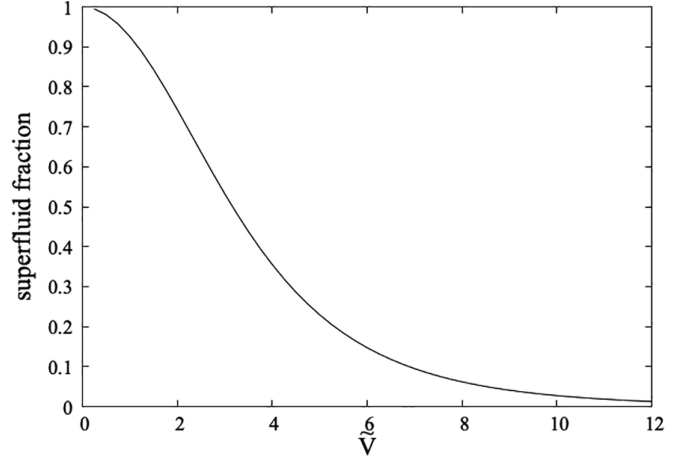


FIG. 2. Superfluid fraction in the 1D lattice as a function of \tilde{V} in the direction of the modulation.

translational inertia [25] as

$$f_s = 1 - \lim_{v_x \rightarrow 0} \frac{\langle \hat{P}_x \rangle}{Nmv_x}, \quad (5)$$

where $\langle \hat{P}_x \rangle = -i\hbar \int \psi^*(\vec{r}) \partial \psi(\vec{r}) / \partial x d\vec{r}$ is the expectation value of the momentum in the x direction of the ^{87}Rb and Nmv_x is the total momentum of the system if all the atoms were moving with the constant velocity v_x .

Alternatively, one could estimate the superfluid fraction using Leggett's formula [5]

$$f_s = \frac{L_x^2}{\int_0^{L_x} dx \langle n(x) \rangle \int_0^{L_x} dx \langle n(x) \rangle^{-1}} \quad (6)$$

where $\langle n(x) \rangle$ is the number density of the ground-state configuration averaged over the transverse $y-z$ directions. The above quantity represents a rigorous upper bound to the superfluid fraction, and it was shown recently that under conditions relevant for most ultracold experiments the two definitions (5) and (6) provide surprisingly close values for the superfluid fraction. We indeed find that the values of f_s from the two definitions above agree with each other to within 1%, in agreement with the findings.

The dependence on \tilde{V} of the superfluid fraction (in the direction parallel to the modulation) is shown in Fig. 2 and the values of f_s for some values of \tilde{V} are given in Table I. We notice that the suppression of the superfluid fraction in the direction of the modulation is quite substantial. In the direction perpendicular to the modulation, i.e., in the y direction, the superfluid fraction is unity in all cases. Therefore, we have a strongly anisotropic superfluid.

A. Single-vortex properties

A linear, singly quantized vortex excitation in the z direction, with the core in the position (x_v, y_v) , can be generated by the “phase imprinting,” i.e., we compute the lowest-energy state obtained by starting the imaginary-time evolution from

the initial wave function

$$\psi_v(\mathbf{r}) = \rho_0^{1/2}(\mathbf{r}) \left[\frac{(x - x_v) + i(y - y_v)}{\sqrt{(x - x_v)^2 + (y - y_v)^2}} \right], \quad (7)$$

where $\rho_0(\mathbf{r})$ is the ground-state density of the vortex-free system. This wave function has unit circulation in the $x - y$ plane and it is orthogonal to the ground state. Such properties are maintained during the imaginary-time evolution until the lowest-energy state with such properties is reached. During this evolution, the vortex position and core structure change to provide at convergence the lowest-energy configuration for a vortex with unit of circulation h/m in the clockwise direction. The sign of the circulation can be changed by changing the sign of the complex i in Eq. (7). We have verified that it is possible to study the dynamics of a vortex also in real time when it is started from a nonstationary position. In fact, in this case we find that the evolution in imaginary time has a rapid transient during which the imprinted phase and modulus of Eq. (7) are modified reflecting the presence of the external potential. During this stage the initial vortex core position is essentially unaffected and it is only for much larger imaginary times that the vortex core position migrates to the nearest equilibrium position. The protocol we follow for real-time study of a vortex is therefore to perform a short imaginary-time evolution and after to evolve the system in real time.

The flow field of a linear vortex has a long-range character $\sim 1/r$, where r is the distance from the position of the vortex core. We have imposed antiperiodic boundary conditions [26] in order that the condition of no flow across the boundary of the computational cell is satisfied [21]. This is equivalent to sum over the phases of an infinite array of vortex-antivortex, i.e., a vortex of opposite chirality is present in each nearest-neighbor cell of the computation cell [27]. Equation (7) can be easily generalized to accommodate a vortex array made of an arbitrary number of vortices and/or antivortices [28]. The case of a pair of vortices with opposite circulation (vortex dipole) will be considered in the following. In the case of a vortex dipole we impose, however, the usual periodic boundary conditions since the flow fields of the two vortices tend to cancel at the cell boundaries.

In general, we find that the stable vortex positions are at the sites of minimum density, i.e., at the locus of maxima of the external potential (see also the following sections, where different types of optical lattices are employed), in agreement with earlier observations [22]. In the case of the present one-dimensional lattice potential the stable positions correspond to the set of lines in the y direction (or better planes if we consider also the z direction) where the density is minimum. Therefore, these lines are at the bottom of a kind of channels along which a vortex can freely move with no change of energy.

The equilibrium vortex structure at one of such sites is shown in Fig. 3 for the case $\tilde{V} = 2$. The streamlines for the velocity field (lines that are tangential to the instantaneous velocity direction) $\vec{v} = \hbar \nabla \phi / m$ (ϕ being the phase of the wave function) are shown in Fig. 4.

Notice the strong deformations with respect to the circular patterns expected from a vortex in a homogeneous system. In order to display these deformations more clearly in Fig. 5 we

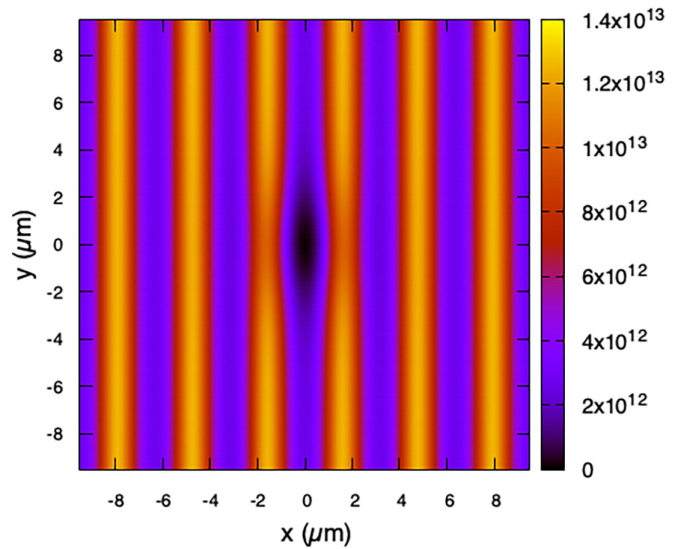


FIG. 3. Structure of a singly quantized vortex at $x = y = 0$, one of the stable sites at the density minimum, for the case $\tilde{V} = 2$. The density is in units of cm^{-3} .

also show the streamlines of the modified phase $\tilde{\phi}$ as defined in Eq. (8) further on. $\tilde{\phi}$ represents the deviation of the phase from the imprinted phase in Eq. (7).

Aside from the stable positions at the bottom of the low-density channels, there are also metastable positions at the density maxima, with higher energy than the equilibrium one. The associated energy barrier for vortex migration from one channel to the neighboring one depends on the amplitude of the modulation.

In Table II the vortex excitation energy and the energy barrier, both per particle and per unit length of the vortex, as well as the angular momentum are reported for selected values

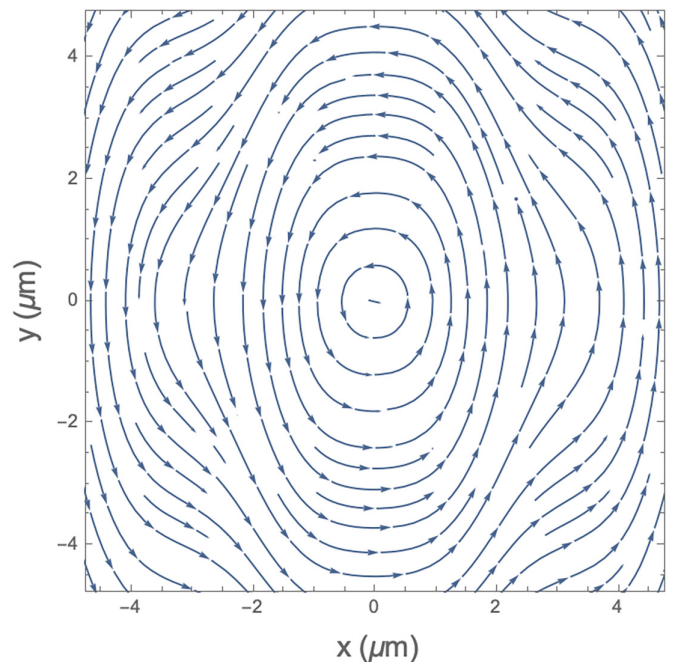


FIG. 4. Streamlines for a vortex in the one-dimensional lattice, for the case $\tilde{V} = 2$. The x and y axes show coordinates in μm .

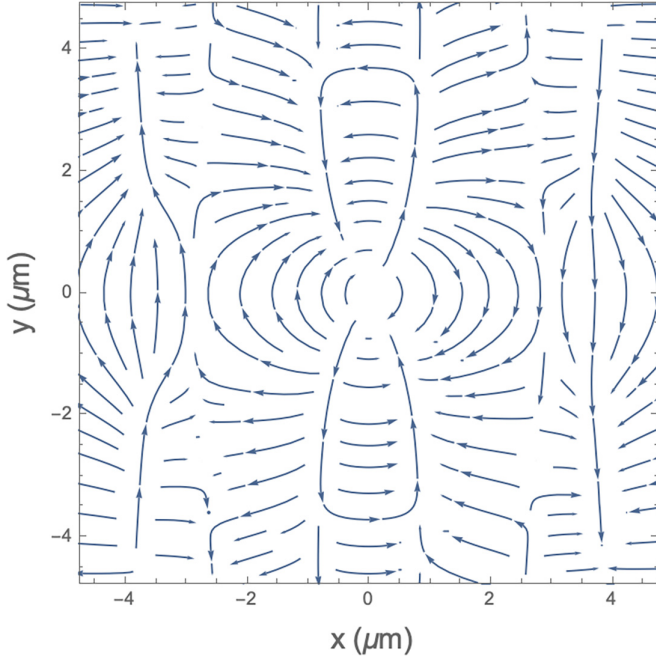


FIG. 5. Streamlines of $\vec{\nabla}\tilde{\phi}$ for a vortex in the one-dimensional lattice, for the case $\tilde{V} = 2$. The x and y axes show coordinates in μm .

of \tilde{V} . The vortex excitation energy ΔE_v is finite because the computation box is finite (in an infinite system ΔE_v would diverge with the size of the system in a logarithmic way). ΔE_v in the modulated system is smaller than in the uniform system and it decreases for increasing \tilde{V} because the vortex core is located in a region where the density decreases as \tilde{V} increases. The energy barrier is a strongly increasing function of \tilde{V} and this reflects the strong variation of the ratio $\rho_{\text{max}}/\rho_{\text{min}}$. We notice also the reduced value of the angular momentum and this reflects the reduced superfluid fraction in presence of the modulation. In the homogeneous state ($\tilde{V} = 0$) the angular momentum deviates from the theoretical value $N\hbar$ due to the boundary effect of the computation box.

B. Vortex dipole properties

Due to the presence of particular stable sites for a vortex caused by the presence of the spatial periodicity imposed by the optical lattice potential, a number of properties are

TABLE II. $\Delta E_v = (E_H - E_0)/L_z$ is the energy (per unit length) cost to create a vortex in the minimum density sites, E_0 being the energy value (per atom) in the absence of the vortex; $(E_B - E_H)/L_z$ is the energy barrier (per unit length) to move a vortex across the maximum density ridge; $\langle \hat{L}_z \rangle$ is the angular momentum along the z axis in units of $N\hbar$.

\tilde{V}	$\Delta E_v/N$ (nK/ μm)	$(E_B - E_H)/N$ (nK/ μm)	$\langle \hat{L}_z \rangle (N\hbar)$
0	0.022		0.925
2	0.018	0.0026	0.788
4	0.011	0.0062	0.492
7	0.005	0.0109	0.198

expected to differ from those in a (nearly homogeneous) superfluid.

In classical hydrodynamics of incompressible fluids, a vortex dipole is a stable entity that moves with a constant velocity that is perpendicular to the plane defined by the vortex axis and the vector \vec{l} joining the vortex and the antivortex core positions and inversely proportional to the distance l between them. The same behavior holds in superfluid systems [1,29] when l is much larger than the healing length, and the vortex dipole propagates with a constant velocity $v_d = \hbar/(ml)$. For example, in the absence of any modulation, a vortex-antivortex pair separated by a distance equal to $l = 4d = 12.7 \mu\text{m}$ is found to translate with a constant velocity $0.058 \pm 0.002 \mu\text{m/ms}$ (the error bar being estimated from the fit to the calculated data), to be compared with the hydrodynamical theoretical value $v_d = 0.057 \mu\text{m/ms}$.

We have studied the real-time evolution of a vortex dipole imprinted in the superfluid in a 1D optical lattice described above. The position of the vortex core is located at each time step by carefully scanning the spatial mesh to find the minimum in the density corresponding to the vortex core. In particular, we will consider two different initial states for the vortex-antivortex pair, i.e., (i) the vortices are located in different minimum energy channels, at initial positions $x = \pm 2d$, where d is the lattice constant; (ii) the vortices are located in the same channel (at $x = 0$), at initial positions $y = \pm 2d$.

In the case (i) we find that the vortex pair moves with a roughly constant velocity, the two vortices remaining in the same initial channel. The translation velocity decreases as the intensity \tilde{V} increases until between 4 and 6 the velocity changes sign, i.e., it is in the opposite direction of motion compared to that of the homogeneous superfluid. This is shown in Fig. 6. Superimposed on the translation is a weak oscillation for small values of \tilde{V} but the oscillation becomes very intense for large values of \tilde{V} , for the largest intensity the motion periodically changes direction. The period of this oscillation becomes shorter for increasing \tilde{V} . For $\tilde{V} = 7$ the period is about 1.9 ms^{-1} . We will discuss more quantitatively the origin of some of these effects in the following.

This behavior of the dynamics of the vortex dipole in distinct channels appears to be quite general: (a) we have verified this when the vortex and the antivortex lie farther apart in channels, (b) when the vortex and the antivortex start with a different y coordinate they rapidly synchronize their motion at a common y coordinate, i.e., they minimize their distance remaining in the initial channels.

A rather peculiar behavior occurs when the initial positions of the two vortices in different channels do not coincide with the stable positions at the density minima, but are rather slightly displaced with respect to it, in opposite directions. During the ensuing dynamics, the vortices are found to move along the channels with complex trajectories shown in Fig. 7. Such trajectories are the result of a uniform translation along the y direction and of two oscillatory motions (occurring with the same frequency) along x and y directions. It should be stressed that this oscillatory motion perpendicular to the direction of translation is not an oscillatory motion around the position of minimum energy but it is rather a one-sided oscillation: if the vortex starts to the right of the minimum at all times it remains on this side of the minimum and it never

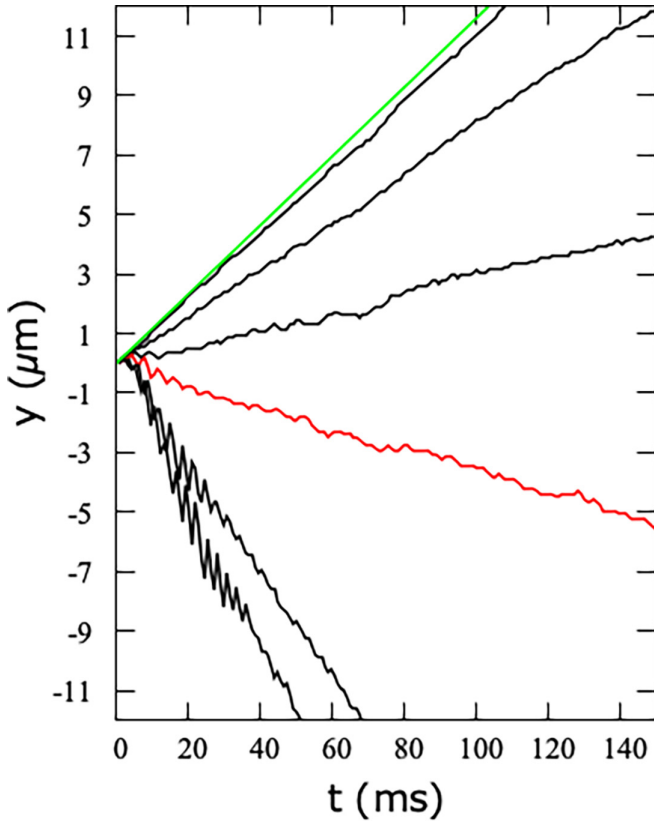


FIG. 6. Trajectories along y of a dipole with the vortices in two different channels. The vortices are initially set at positions $x = \pm 2d$ and with the same y . The y coordinates of the two vortices of the dipole remain equal at all times within the grid of the computation. From top to bottom: $\tilde{V} = 0, 1, 2, 3, 4, 6, 7$.

crosses to the other side. The same holds if it starts to the left. Therefore, this dynamics is quite distinct from that of a massive particle moving around a minimum energy position.

We note that small-amplitude oscillations superimposed to vortex trajectories have been found in a two-component Bose mixture [30], within the so-called massive point-vortex model, for a single vortex with a rigid circular boundary, where a massless vortex can only precess uniformly. This phenomenology and the one unveiled by our calculations certainly share some common physical properties. The model of Ref. [30] is based on a Lagrangian formulation for point vortices, and has been applied so far to homogeneous systems [30,31]. It might be of great interest to extend such model to the case of nonhomogeneous systems like the one described here.

In the case (ii), vortex and antivortex started in the same channel, for $\tilde{V} = 4, 7$ the two vortices move towards one another, remaining in the same channel, until they annihilate at the origin, as shown in Fig. 8. However, in the case of a less modulated structure ($\tilde{V} = 2$), they remain initially in the same channel and move towards one another until they nearly touch at time $t = 32$ ms (still being in the density minimum same channel): at this point, they appear to repel each other and jump to the next channel, annihilating there at a later time. We notice that a similar behavior has been observed in experiments [9], where vortices in BEC are found

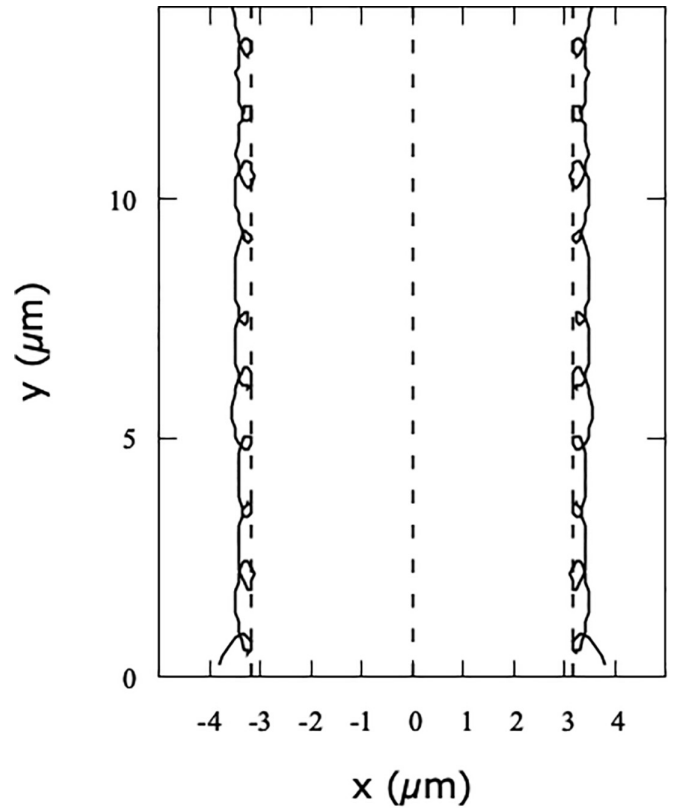


FIG. 7. Dynamics of a vortex dipole when the initial vortex positions are slightly displaced with respect to the channel axis. The three vertical lines show the loci of minimum density. The simulation refers to the case $\tilde{V} = 2$.

to approach each other so closely that they appear to coalesce, but then move away from each other after the close encounter. This combination of jump and approach of the vortex pair two vortices of the dipole has some similarity with what we find in the case of 2D modulations as described in the next subsection.

From the equation for the velocity of a vortex within the GP equation we can understand at a qualitative level some aspects of our results. The flow field of one vortex on the other is in the transverse direction of the channel, i.e., in the region where the density of the superfluid is increasing. This variation of density gives rise to a component of the velocity of the vortex in the longitudinal direction along the bottom of the channel. Following Ref. [32] (see also Ref. [25]) one may write the vortex wave function $\psi_v(\vec{r}, t)$ with the core located at position \vec{r}_0 at time t as

$$\psi_v(\vec{r}, t) = (x + iy - x_0 - iy_0)\tilde{\rho}e^{i\tilde{\phi}} \quad (8)$$

[here $\vec{r}_0 = (x_0, y_0)$ is expressed in complex notation as $z_0 = x_0 + iy_0$], where the factor $z = x + iy - x_0 - iy_0$ represents the ideal gas vortex wave function and $\tilde{\rho}(\vec{r}, t)$ and $\tilde{\phi}(\vec{r}, t)$ represent the deviations of the modulus and of the phase from this ideal gas form (see Ref. [32] for additional details). Several effects contribute to the deviation of the vortex wave function from the ideal gas form, i.e., $\tilde{\rho}(\vec{r}, t)$ and $\tilde{\phi}(\vec{r}, t)$ have the contribution due to the presence of other vortices, to the effect of an external potential and, finally, to the deviation of $\psi_v(\vec{r}, t)$

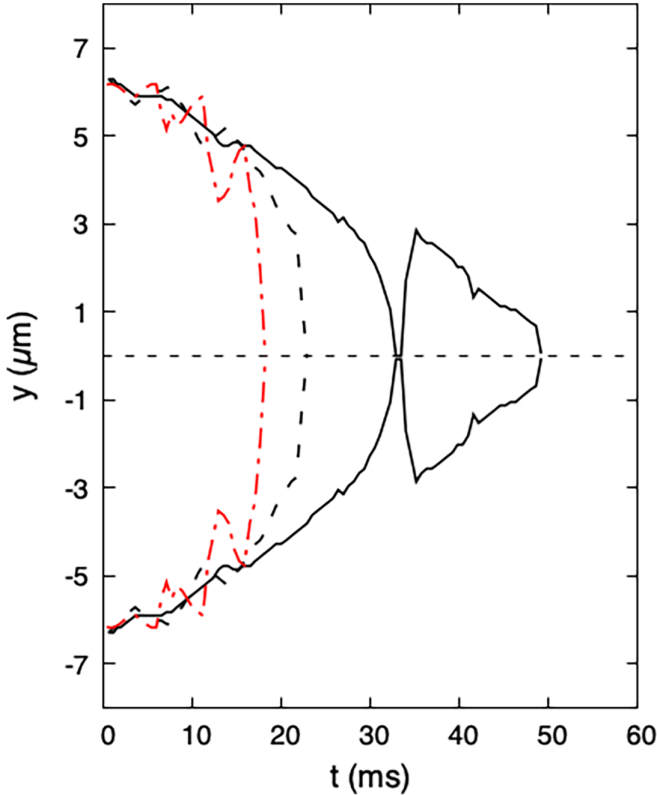


FIG. 8. Trajectories along y of the two vortices of a dipole started in the same channel. The vortices are initially set at positions $y = \pm 2d$. From left to right $\tilde{V} = 7, 4, 2$.

from the ideal gas form caused by the interatomic interactions. On the basis of the Gross-Pitaevskii equation here adopted the velocity of the vortex is [32]

$$\vec{v} = \frac{\hbar}{m} (\nabla \tilde{\phi} - \hat{k} \times \nabla \ln \tilde{\rho}), \quad (9)$$

where the vector \hat{k} is the unit vector in the direction of the circulation, i.e., in the z direction in the present case. As soon as the vortex position moves out of the bottom of the channel the second contribution to the velocity in Eq. (9) becomes nonzero due to the increasing density and its gradient is in the x direction. The vector product of these two vectors is in the y direction and points toward the other vortex. Therefore, the velocity of one vortex of the pair has one longitudinal contribution from the external potential and a transverse contribution from the gradient of the phase due to the other vortex of the pair. This transverse term might dominate if the amplitude of the external potential is weak enough so that the vortex pair could move across channels but in any case due to the longitudinal contribution the two vortices move also against each other until they annihilate. The longitudinal contribution to the vortex velocity might dominate for large amplitude of the external potential so that the two vortices remain in the starting channel until annihilation. Equation (9) for the velocity of the vortex core also explains why we see one-sided oscillations of the vortex: the gradient of the local density tends to bring the vortex core toward the minimum

density position but at this minimum this contribution to the velocity vanishes.

It should be noticed at this point that Eq. (9) is not a self-contained equation for the dynamics of a vortex because the tilded quantities are just a different way to represent the solution of the time-dependent GP equation. As such, Eq. (9) can help to develop qualitative arguments as exposed above, but it cannot predict the dynamics unless approximations are introduced.

On the basis of Eq. (9) for the velocity of a vortex we can also understand why the translation velocity of the vortex dipole lying in two different channels is reduced with respect to the homogeneous case. In fact, from Fig. 5 one can see that the direction of $\nabla \tilde{\phi}$ along the line corresponding to $y = 0$ has the opposite direction of the one of the homogeneous case, i.e., it points downward for $x > 0$ and upward for $x < 0$ and not vice versa as should be for a positive circulation vortex in a homogeneous superfluid. This means that the induced velocity due to the other vortex of the dipole is reduced compared with the value for the homogeneous system. Why the translation velocity even changes direction at large modulations and a longitudinal oscillation is present, however, cannot be explained by these simple considerations.

C. Single vortex in a trap

An important question is if the oscillations in the dynamics of a vortex pair displayed in Fig. 7 are a consequence of the mutual coupling between vortex-antivortex or are rather a property of the single vortex. We therefore considered the dynamics of a single vortex initially imprinted in a position slightly displaced from a position of minimum energy by the same amount as in the dipole simulation just described. However, boundary effects mask the genuine dynamics in the case of an extended system with antiperiodic boundary conditions. To avoid this we used instead a finite system confined in the $x - y$ plane by an additional circular “box” potential of the form

$$V_{\text{box}}(x, y) = U_0 \left[1 - \frac{1}{e^{(R-R_0)/\sigma} + 1} \right], \quad (10)$$

where $R = \sqrt{x^2 + y^2}$, R_0 is the chosen value for the radius of the circular trap. We chose the following values: $R_0 = 14.3 \mu\text{m}$, $U_0 = 60 \text{ nK}$, and $\sigma = 0.212 \mu\text{m}$. With such choice, the potential V_{box} becomes different from zero as R approaches R_0 and rapidly becomes very repulsive reaching the value U_0 . As a result, the system is essentially unaffected in the inner region by this potential, where the system density is very close to that of the extended system, and goes exponentially to zero for radial distances from the center larger than R_0 . We chose the number of atoms so that the density pattern in the interior of the circular trap is very similar to that of the extended system, for a given value of \tilde{V} .

We perform the computation with the external potential $V(\vec{r}) = V_{\text{OL}}(x, y) + V_{\text{box}}(x, y)$ and V_{OL} is such that the center of the trap is a maximum of the OL, i.e., the center of the trap is an equilibrium position for the vortex core. We find that the vortex remains immobile if initially it is located at or very near the center of the trap, in the low-density channel passing through it. If the initial position of the vortex is off

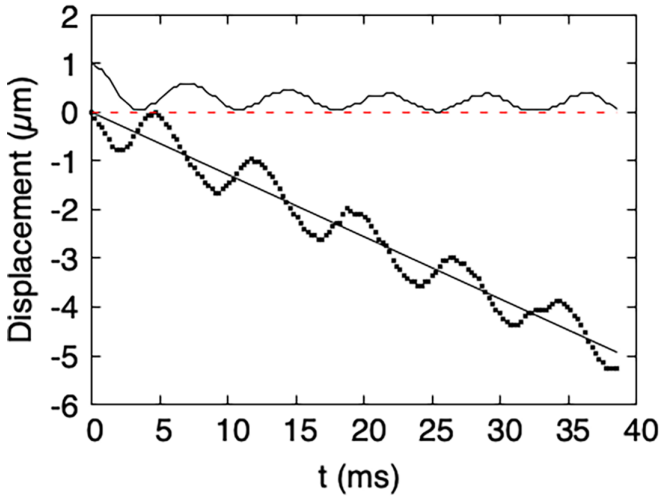


FIG. 9. Upper curve: displacement $x(t)$ of the vortex core perpendicular to the channel axis; lower curve: displacement $y(t)$ of the vortex core parallel to the channel axis. The dotted line shows a least-square fit to $y(t)$. The simulation refers to the case $\tilde{V} = 2$.

center along the y direction by a larger amount, however, the vortex is found to migrate towards the edge of the trap and disappears once it approaches the trap edge.

When the initial position is at $y = 0$ but slightly off center along the x direction, i.e., away from an equilibrium position, then the vortex moves toward the border of the trap and the radial motion is the superposition of a uniform motion in the radial direction and of a longitudinal and transverse oscillatory motion, similarly to the case of a vortex dipole shown in Fig. 7. As in the case of the vortex dipole the oscillatory motion is one sided: the vortex never crosses the line of minimum density but it remains on the same side of the channel from which it started. This is shown in Fig. 9.

We have estimated, from the trajectories $x(t)$ and $y(t)$, the frequency characterizing these oscillations, which is reported in Fig. 10 as a function of \tilde{V} , together with the average translation velocity of the vortex along the channel.

We finally note that the frequencies found for the oscillations of a single vortex, as discussed above, agree with the ones found for the case of a vortex dipole propagating in parallel channels. We have checked the effect of changing the density of the system on the oscillation frequency in Fig. 10. We thus studied the dynamics of a vortex slightly displaced from the equilibrium position in the transverse direction x , as described before, but when the total number of atoms in the system is doubled (halved). We find that both the amplitude and frequency of the transverse oscillations are unaffected by the increased (decreased) density. Also, the frequency of the back-and-forth oscillations along the channel axis is not changed, whereas its amplitude is reduced as the density increases.

A natural question is if these oscillations might be due to the coupling of the vortex motion with the phonon excitations in the system which can be created by the vortex motion through the system. However, this is not the case. In fact, we have computed, by using the Bogoliubov–de Gennes approach, the dispersion relation perpendicular and parallel to

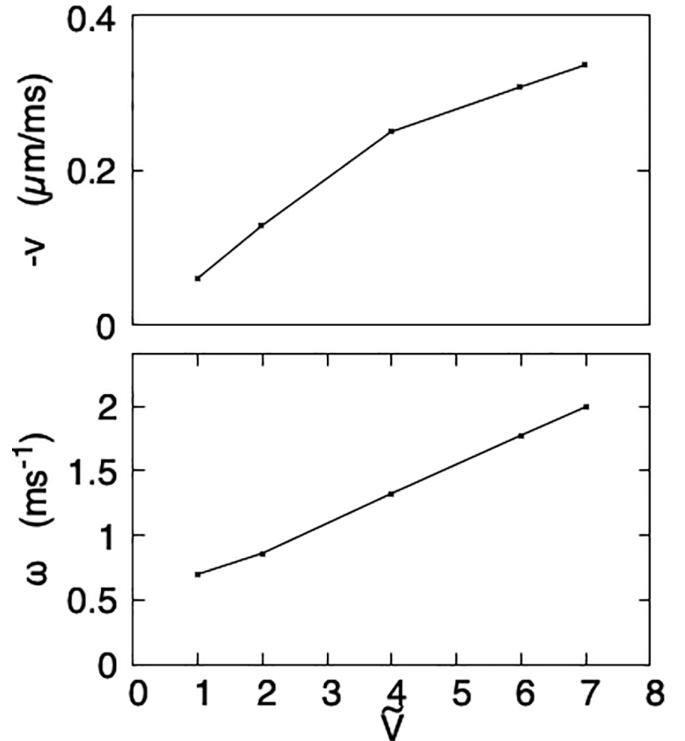


FIG. 10. Upper panel: average translation velocity of a single vortex starting from a slightly displaced x position from the center of the trap. Lower panel: calculated frequency of the oscillations occurring during the vortex motion along the channel.

the channel direction. The phonons propagating in a direction perpendicular to the channels, having a dispersion relation which flattens at the Brillouin zone boundary, are those with the highest density of states. Their frequencies are found to be [33] in the range $0.12 < \omega < 0.4 \text{ ms}^{-1}$ (corresponding to the range $7 > \tilde{V} > 2$), i.e., much smaller than the observed vortex oscillation frequencies.

IV. ^{87}Rb IN 2D OPTICAL LATTICE

A. Square lattice

The external potential $V(\vec{r})$ acting on the Rb atoms is taken in the form of a periodic potential with square symmetry, i.e., $V(\mathbf{r}) = V_{\text{OL}}(x, y)$, where

$$V_{\text{OL}}(x, y) = V_0[\cos^2(\kappa x) + \cos^2(\kappa y)]. \quad (11)$$

As done in the previous sections, the optical potential strength V_0 is expressed in the following in terms of an adimensional quantity \tilde{V} such that $V_0 = \tilde{V} \times 10^{-14} \text{ Ha} = \tilde{V} \times 3.158 \text{ nK}$.

We first computed the ground-state in the presence of the periodic potential V_{OL} , for different values of the amplitude \tilde{V} . We will use in the following a shorthand notation where the site of maximum density (corresponding to the minimum of the lattice potential) is called “top” (T), the site with minimum density (corresponding to the maximum of the lattice potential) is called “hollow” (H), and the saddle point between two adjacent top sites is called “bridge” (B).

As in the case of the 1D potential discussed in Sec. III, the system is superfluid, with a superfluid fraction f_s which

TABLE III. \tilde{V} is the amplitude of the periodic potential. The density values at the hollow, top, and bridge sites are shown; μ is the chemical potential; f_s is the superfluid fraction computed from the nonclassical translational inertia.

\tilde{V}	ρ_H (cm $^{-3}$)	ρ_T (cm $^{-3}$)	ρ_B (cm $^{-3}$)	μ (nK)	f_s
0	6.943×10^{12}	6.943×10^{12}	6.943×10^{12}	2.584	1
2	2.797×10^{12}	1.338×10^{13}	6.462×10^{12}	8.48	0.929
4	0.9412×10^{12}	2.079×10^{13}	5.295×10^{12}	13.57	0.768
7	0.1668×10^{12}	3.151×10^{13}	3.329×10^{12}	19.97	0.513
9	0.0537×10^{12}	3.793×10^{13}	2.288×10^{12}	23.59	0.375

depends on the amplitude of the lattice modulation V_0 . The relevant densities at the various lattice sites and the calculated superfluid fraction are reported in Table III.

B. Vortices

We imprint a single vortex using the procedure described before. If the vortex initial position is in a generic point of the unit cell of the modulating potential, during the imaginary-time evolution the vortex core moves to the closest minimum density position. We find that stable vortex positions are at the low-density sites corresponding to the maxima of the optical potential (hollow site), as discussed in the following. In the case of a square lattice these equilibrium positions have the same square symmetry. The vortex structure at the hollow site is shown in Fig. 11 for the case $\tilde{V} = 2$.

We show in Fig. 12 the equilibrium vortex structure for different values of the potential depth \tilde{V} , including the value $\tilde{V} = 0$. In order to improve the visualization of the vortex core structure, we show in the figures the density differences with respect to the configuration without vortex.

We show in Fig. 13 the calculated vortex excitation energy per unit length $\Delta E_v \equiv (E_v - E_0)/L_z$ as a function of density of Rb atoms.

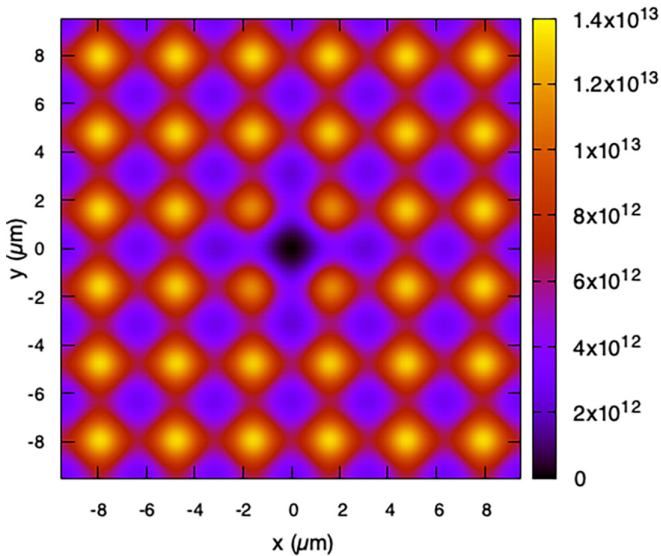


FIG. 11. Structure of a singly quantized vortex in the stable hollow site, for the case $\tilde{V} = 2$. The vortex core is at the origin ($x = y = 0$). The density is in units of cm $^{-3}$.

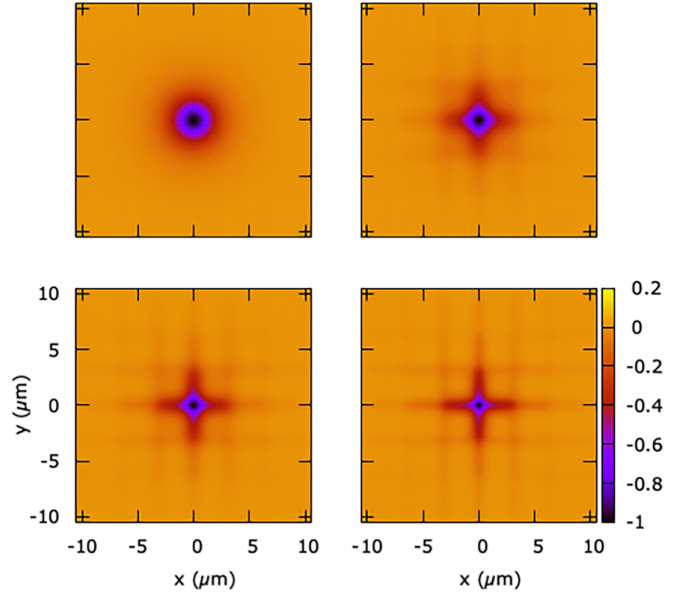


FIG. 12. Relative density difference $(\rho_{\text{vort}} - \rho_{\text{novort}})/\rho_{\text{novort}}$ showing the minimum energy vortex structure (hollow site) for $\tilde{V} = 0, 2, 4, 7$.

Notice the decrease of the vortex energy, for a given N , with the modulation amplitude of the lattice potential. This is a consequence of the decreasing density in the region of the vortex core as \tilde{V} increases.

The streamlines around the vortex core are shown in Fig. 14 for $\tilde{V} = 7$.

Aside from the stable position at the hollow site, we have found that the saddle point between two adjacent density minima (*bridge site* in the following) is a metastable equilibrium position for a vortex, with slightly higher energy than the equilibrium one. A third metastable position for the vortex is found, at least for not too large value of \tilde{V} , at the high-density sites (*top site* in the following), corresponding to the minima of the optical potential. We show the vortex structures for

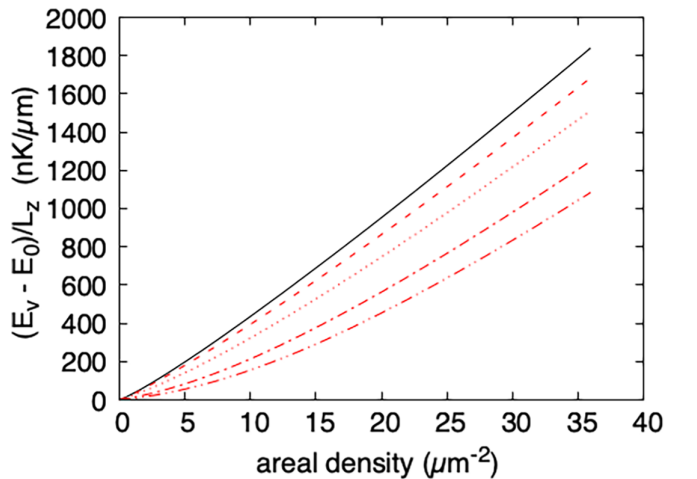


FIG. 13. Vortex total energy as a function of the areal density of Rb atom. From top to bottom: $\tilde{V} = 0, 2, 4, 7, 9$. The density $n_a = 9.92 \mu\text{m}^{-2}$ is the one used in most of the calculations discussed in the paper.

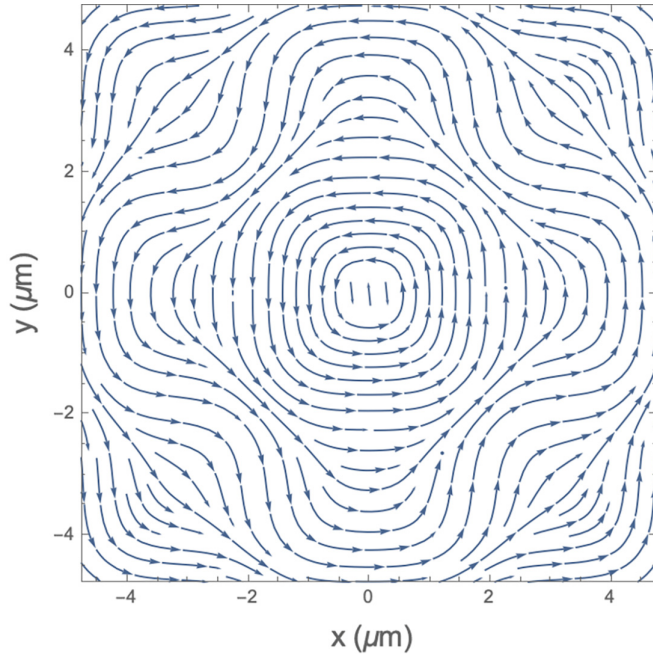


FIG. 14. Streamlines for a vortex in the hollow site, for the case $\tilde{V} = 7$. The x and y axes show coordinates in μm .

these configurations in Fig. 15, together with the stable hollow configuration.

In a uniform superfluid the energy of a vortex does not depend on the position of its core so that it is free to move under the influence of a perturbation. Our results show that in presence of a 2D optical lattice the vortex energy becomes a

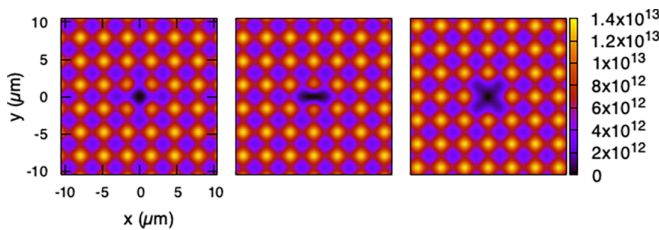


FIG. 15. Structure of a singly quantized vortex, for the case $\tilde{V} = 2$ (only a portion of the density in the $x - y$ plane is shown). From left to right: (i) hollow (most stable) site; (ii) bridge site; (iii) top site. The density is in units of cm^{-3} .

TABLE IV. $\Delta E_v = (E_H - E_0)/L_z$ is the energy (per unit length) cost to create a vortex in the minimum density (hollow) sites, E_0 being the energy value (per atom) in the absence of the vortex; $\langle \hat{L}_z \rangle$ is the angular momentum along the z axis in units of $N\hbar$ (the value at $\tilde{V} = 0$ denoted with an asterisk has been computed with a bigger cell, with a surface area in the $x - y$ plane four times larger the one used for all the calculations); $(E_B - E_H)/L_z$ and $(E_T - E_H)/L_z$ are the energy barriers (per unit length) to move a vortex across the bridge site and the top site, respectively.

\tilde{V}	$\Delta E_v/N$ (nK/ μm)	$(E_B - E_H)/N$ (nK/ μm)	$(E_T - E_H)/N$ (nK/ μm)	$\langle \hat{L}_z \rangle$ ($N\hbar$)
0	0.0220	—	—	0.925(0.927*)
2	0.0199	0.00049	0.00210	0.858
4	0.0163	0.00046	0.00468	0.708
7	0.0108	0.00026	0.00886	0.486
9	0.0078	0.00019	0.01147 (unstable)	0.356

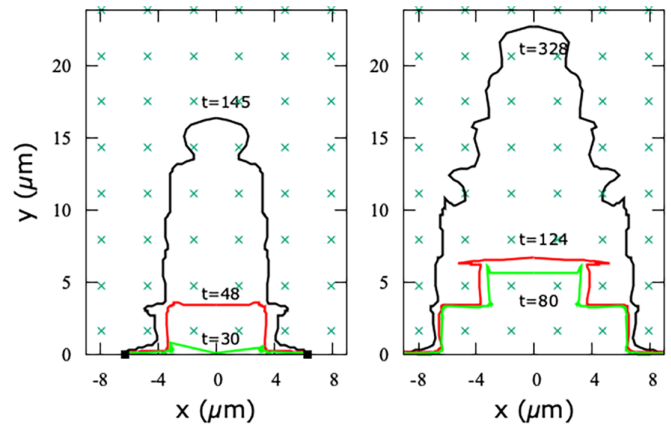


FIG. 16. Trajectories of the two vortices of the dipole in the $x - y$ plane ending in vortex dipole annihilation. Left panel: the two vortices are initially placed at $x = \pm 2d = \pm 6.35 \mu\text{m}$. From top to bottom: $\tilde{V} = 2, 4, 7$. The label on each trajectory gives the observed annihilation time in milliseconds. The crosses show the positions of the T sites where the Rb density is maximum. Right panel: the two vortices are initially placed at $x = \pm 3d = \pm 9.53 \mu\text{m}$.

periodic function of position. The associated energy barriers for vortex migration along the lattice are reported in Table IV. These barriers will play an important role, as discussed in the following, in the dynamics of vortices across the lattice.

C. Vortex dipole properties

Following the protocol described in Sec. III B we imprint a vortex dipole in the 2D modulated superfluid and follow its real-time dynamics. Instead of rigidly translating as in an homogeneous superfluid phase, in the presence of spatial modulation the vortex and antivortex approach each other by a series of jumps from one site to another moving mostly across the saddle positions until they annihilate in a very short time and their energy is released in the form of density wave excitations.

The path followed during the annihilation process depends on the amplitude \tilde{V} of the optical lattice: the smaller the modulation, the farther the dipole moves along the y direction before annihilation, and the longer it takes for the dipole to disappear. This is shown in Fig. 16, where it appears that the vortex hopping occurs mostly across bridge sites. The two vortices are initially placed at $x = \pm 2d = \pm 6.35 \mu\text{m}$ (left

panel of Fig. 16). In the right panel of Fig. 16 the annihilation paths are shown instead when the two vortices are initially placed at a larger mutual distance, $x = \pm 3d = \pm 9.53 \mu\text{m}$. We recall that in absence of OL the vortex dipole would move rigidly with constant velocity in the y direction.

It is of interest a comparison with the dynamics of a vortex dipole in the supersolid state of dipolar bosons [21]. There is some similarity with what we find here in that the vortices of the dipole move by approaching each other by jumps between equilibrium sites with final annihilation but the studied case for dipolar atoms did not show any translation of the dipole in the direction perpendicular to the line joining the vortices.

The energy released immediately after the annihilation goes into excitations of the system. In order to gain some insights on the character of the excitations we computed the spectral density of the kinetic energy of the superfluid velocity field, decomposing it into compressible and incompressible parts [34–36]. Briefly, one splits the density-weighted velocity field $\vec{u}(\vec{r}, t) \equiv \sqrt{\rho(\vec{r}, t)}\vec{v}(\vec{r}, t)$ into a compressible (C) and an incompressible (I) part, $\vec{u}(\vec{r}, t) = \vec{u}^I(\vec{r}, t) + \vec{u}^C(\vec{r}, t)$, such that $\vec{\nabla} \cdot \vec{u}^I(\vec{r}, t) = 0$ and $\vec{\nabla} \times \vec{u}^C(\vec{r}, t) = 0$. One can therefore decompose the kinetic energy E into two parts, $E = E^I + E^C$, where

$$E^{I,C} = \frac{m}{2} \int d\vec{r} |\vec{u}^{I,C}(\vec{r}, t)|^2. \quad (12)$$

The compressible component is attributed to the kinetic energy contained in the sound field, while the incompressible part gives the contribution from quantum vortices.

In \vec{k} space, the total incompressible (compressible) kinetic energy $E^{I,C}$ is given by

$$E^{I,C} = \frac{m}{2} \sum_{j=x,y} \int d^2\vec{k} |F_j(\vec{k})|^2, \quad (13)$$

where

$$F_j(\vec{k}) = \frac{1}{2\pi} \int d^2\vec{r} e^{-i\vec{k}\cdot\vec{r}} u_j^{I,C}(\vec{r}) \quad (14)$$

(the time dependence is implied).

The one-dimensional spectral density in k space is given by integrating over the azimuthal angle

$$E^{I,C}(k) = \frac{mk}{2} \sum_{j=x,y} \int_0^{2\pi} d\phi_k |F_j(\vec{k})|^2. \quad (15)$$

We show in Fig. 17 the spectral density of the kinetic energy $E^{I,C}(k, t)$ for the case $\tilde{V} = 4$, when the two vortices are initially placed at positions $x = \pm 2d$ (whose trajectories are displayed in the left panel of Fig. 16). The horizontal arrows show two relevant wave vectors: $k_{vv} = 2\pi/l$, where l is the initial vortex-vortex distance, and $k_d = 2\pi/d$, which is the wave vector corresponding to the periodic modulation with lattice constant d . The lower panel clearly shows the sharp transition when the vortices disappear with a strong drop of the incompressible kinetic energy. The peak in the incompressible part appearing below the wave vector k_{vv} before annihilation is a general feature also found in the calculations for a vortex dipole in Ref. [36] (see in particular the Fig. 3 of that reference). After vortex annihilation the compressible part (upper panel) starts showing features connected to density fluctuations (sound waves). One can notice that also before

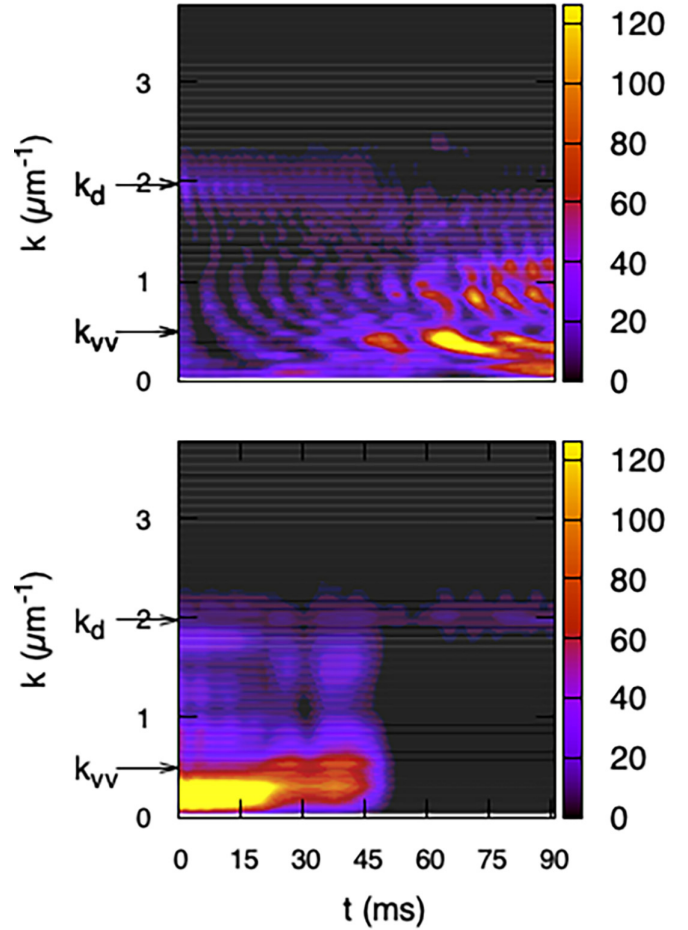


FIG. 17. Kinetic energy spectra for the case $\tilde{V} = 4$, square OL. Top: compressible part; bottom: incompressible part.

vortex annihilation a faint time modulation is present over an extended range of k vectors and its period is about 7 ms. We have computed [33] the phonon frequencies of the Rb gas in presence of the 2D OL but without vortices and find that this 7-ms period falls inside a gap of the phonon spectrum. The vortex dipole represents a defect in the modulated system and our interpretation of this oscillation is in terms of a localized vibration of the Rb gas around the moving vortex dipole.

We have also considered two other types of 2D lattices, with triangular symmetry and with the honeycomb structure. Similarly with what we have done in the case of the square lattice, we studied the vortex structures in such lattices and the real-time dynamics of a vortex-antivortex pair, eventually leading to annihilation as the vortices meet. The results are reported in the Supplemental Material [37].

D. Visualizing vortices in optical lattices

As previously discussed, the direct visualization of vortices in the system studied here might be difficult, especially for large values of the amplitude of the OL. This is a consequence of the fact that the vortex cores tend to localize in the low-density sites of the periodic lattice. We suggest here that a simple way to visually detect the presence of vortices in the

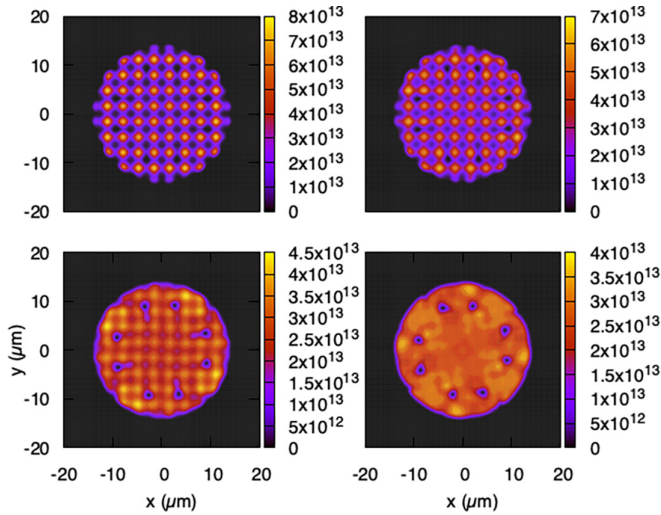


FIG. 18. From left to right, from top to bottom: panel (i): density of the stationary state in the corotating frame, for $\tilde{V} = 7$; (ii)–(iv): density patterns at $t = 1.6, 4.1,$ and 6.4 ms, during the time evolution of the state (i) when the amplitude \tilde{V} is ramped linearly to zero in 5 ms. The density is in units of cm^{-3} .

modulated system can be achieved by sudden removal of the optical lattice potential.

One way to experimentally cause vortex nucleation is by means of rotation of the optical lattice. We consider here the case of the square lattice with the same radial confining potential (circular “box”) used to analyze the dynamics of a single vortex in the one-dimensional lattice described in Sec. III C.

To enforce rotations (with some fixed angular velocity ω , around the z axis) we work in the corotating frame, described by the Hamiltonian

$$\{H - \hbar\omega\hat{L}_z\} \Psi(\mathbf{r}) = \mu \Psi(\mathbf{r}), \quad (16)$$

where \hat{L}_z is the total angular momentum operator in the z direction and H is the Hamiltonian of Eq. (2).

We first compute the stationary state in the presence of a rotation of the system with constant ω by solving the Euler-Lagrange equations in imaginary time associated with the previous Hamiltonian. If the imposed angular velocity is large enough (i.e., larger than the critical frequency for a single vortex nucleation), a number of vortices will eventually populate the system, which may later be visualized. These vortices, as it happens in rotating finite superfluid samples, are initially nucleated on the boundaries of the system, and rapidly settle to an equilibrium position at a distance from the center which depends on the value of the rotational frequency: the larger the latter is, the closer to the center will be the vortices in the stationary-state configuration.

As an example, we show in the first panel of Fig. 18 the stationary state obtained with $\omega = 2\pi \times 8$ Hz in presence of a square OL with value $\tilde{V} = 7$. At first sight, the resulting density profile resembles that of the ground state in the absence of rotation. However, a finite value for \hat{L}_z indicates the presence of vorticity in the system.

A possible way to increase the vortex visibility is to rapidly remove the periodic potential (but keeping the radial

confinement active) so that the system may evolve towards a more homogeneous state where the increased contrast between the empty core and the background density may allow to reveal the vortex positions.

We therefore perform a real-time dynamics, starting from the stationary state shown in the first panel of Fig. 18, with a linear ramp of the optical potential which brings its value from $\tilde{V} = 7$ to 0 in 5 ms. The three panels (from left to right, from top to bottom) of Fig. 18 show snapshots of the Rb density during the real-time evolution, clearly showing a ring of six vortices as the density modulations are suppressed. Notice that the vortex core positions rotate with the imposed angular velocity ω .

We remark that the time required to visually disclose the vortex cores is so short that the final core positions (last panel in the figure) coincide with their initial positions in the modulated phase shown in the first panel. Such short times exclude the possibility that vortices are nucleated during the quench from the modulated to the homogeneous phase.

V. CONCLUSIONS

We have studied the superfluid phase of boson ^{87}Rb atoms under the influence of an optical potential which induces a spatial modulation of the local density. The main interest is on the static and dynamical properties of vortex excitations. We have studied the system at zero temperature with the mean field Gross-Pitaevskii equation and our investigation is mainly on the regime of strong modulation when the excursion between low and high density becomes quite large. We study the system in a flat geometry so that one can neglect the transverse direction and the system is close to the 2D limit. The dynamics of a vortex in an almost 2D superfluid is rather simple when no other vortex is present within its healing length: the core moves with the gradient of the phase due to other vortices. Consequences of this law are, for instance, that a vortex dipole is a stable entity and it rigidly translates with constant velocity and that one vortex in a circular trap performs a precession around the trap center. Deviations from such behaviors in a weakly inhomogeneous superfluid have been studied by a number of authors as discussed in the Introduction. We have studied a rather different regime, when the inhomogeneity is very large. In presence of an intense optical potential we find a vortex behavior quite different from that of the uniform superfluid. Depending on the symmetry of the optical lattice two vortices of opposite chirality, a vortex dipole, can move by jumps approaching each other until annihilation with a lifetime of the pair depending on the intensity of the optical lattice or the vortices of the dipole do translate but with a velocity even of opposite direction of that present in the uniform case and, in addition, this translation takes place together with an oscillatory motion. Or a single vortex in a trap does not perform a precessional motion but it moves toward the periphery of the trap with a complex motion consisting of translation of an oscillation. These periodic motions are single side in the sense that they never cross the equilibrium position from the starting place, a behavior quite different from that of a massive particle around an equilibrium position. Such

features of the vortex motion derive from two facts. On one hand, the vortex energy depends on the local density at the position of its core and the energy is lowest where the density has a minimum, i.e., at the positions of the maxima of the optical lattice. A consequence of this is that a vortex is not free to move but it is pinned to specific sites or lines depending on the symmetry of the optical lattice. On the other hand, the stream lines have large deviations from the simple circular shape of the uniform superfluid. The superfluid fraction is reduced from unity, even if our system is at zero temperature, and this reduction can be quite large for large amplitudes of the optical potential. In the case of 1D optical potential the superfluid has a stripe structure and the superfluidity is very anisotropic: the superfluid fraction is unity along the stripes and it is reduced in the direction perpendicular to the stripes. At the same time a vortex has a unit circulation but a reduced angular momentum compared to that of a uniform superfluid.

It is possible now to generate experimentally vortex dipoles in a superfluid of cold atoms [11] so it should be possible to verify our predictions for the dynamics of vortices in a modulated superfluid. We have studied the case of ^{87}Rb atoms but our results should be valid for other bosons with positive scattering length. The jumping behavior and annihilation of a vortex dipole seen in the case of a 2D optical lattice have some similarity with that of a vortex dipole in a supersolid [21].

Our study is based on a mean field theory and we should pose the question of the accuracy of such theory because it is known that a Mott transition to a localized state sets in when the optical lattice is strong enough [38]. In terms of recoil energy the amplitude of the optical potential in our study is much smaller than the amplitudes for which experimentally

the localization has been found to set in. In addition, we have indication of the internal consistency of the used theory because we have performed computations [33] of the excitation spectrum of our system with the Bogoliubov–de Gennes equation and no sign of instability has been found. This gives confidence on our theoretical results.

We have been able to explain at a qualitative level some aspects of our results like the approach of the two vortices of a dipole or the one-sided oscillations in terms of the expression of the velocity of the vortex core and its relation to the gradient of the local density of the superfluid.

One would like to see a treatment of the systems of our study on the basis of an approximate analytic treatment like a suitable extension of the point-vortex approximation as explored in Ref. [32]. Different extensions of this study come to mind. One is the study of vortices in the supersolid phase of soft-core bosons or in supersolid with a stripe structure. The flat geometry used in our computations does not allow flexural motion of the core of the vortex. Of interest will be a similar study when the system is extended in the third direction and key questions are the fate of the Kelvin waves that characterize the motion of a vortex core in 3D [1] or if additional excitations are present similar to kinks of a dislocation in a solid. Theory predicts that a supersolid phase with a stripe structure can be present with dipolar bosons [39]. Our results for the vortex behavior in a 1D modulated system should be relevant also for such supersolid system.

ACKNOWLEDGMENT

We thank G. Roati, A. Burchianti, and A. Richaud for useful discussions.

-
- [1] R. J. Donnelly, *Quantized Vortices in Helium II* (Cambridge University Press, Cambridge, 1991).
 - [2] A. L. Fetter, *Rev. Mod. Phys.* **81**, 647 (2009).
 - [3] S. Burger, F. S. Cataliotti, C. Fort, P. Maddaloni, F. Minardi, and M. Inguscio, *Europhys. Lett.* **57**, 1 (2002); F. S. Cataliotti, S. Burger, C. Fort, P. Maddaloni, F. Minardi, A. Trombettoni, A. Smerzi, and M. Inguscio, *Science* **293**, 843 (2001).
 - [4] J. Tao, M. Zhao, and I. B. Spielman, *Phys. Rev. Lett.* **131**, 163401 (2023).
 - [5] A. J. Leggett, *Phys. Rev. Lett.* **25**, 1543 (1970); *J. Stat. Phys.* **93**, 927 (1998).
 - [6] S. Moroni, F. Ancilotto, P. L. Silvestrelli, and L. Reatto, *Phys. Rev. B* **103**, 174514 (2021).
 - [7] L. Chomaz, I. Ferrier-Barbut, F. Ferlaino, B. Laburthe-Tolra, B. L. Lev, and T. Pfau, *Rep. Prog. Phys.* **86**, 026401 (2023).
 - [8] T. Isoshima, M. Nakahara, T. Ohmi, and K. Machida, *Phys. Rev. A* **61**, 063610 (2000); K. C. Wright, L. S. Leslie, A. Hansen, and N. P. Bigelow, *Phys. Rev. Lett.* **102**, 030405 (2009).
 - [9] T. W. Neely, E. C. Samson, A. S. Bradley, M. J. Davis, and B. P. Anderson, *Phys. Rev. Lett.* **104**, 160401 (2010).
 - [10] Y.-J. Lin, R. L. Compton, K. Jimenez-Garcia, J. V. Porto, and I. B. Spielman, *Nature (London)* **462**, 628 (2009).
 - [11] W. J. Kwon, G. Del Pace, K. Khani, L. Galantucci, A. M. Falconi, M. Inguscio, F. Scazza and G. Roati, *Nature (London)* **600**, 64 (2021).
 - [12] P. G. Kevrekidis, R. Carretero-González, G. Theocharis, D. J. Frantzeskakis and B. A. Malomed, *J. Phys. B: At. Mol. Opt. Phys.* **36**, 3467 (2003).
 - [13] D. S. Goldbaum and E. J. Mueller, *Phys. Rev. A* **77**, 033629 (2008).
 - [14] H. Pu, L. O. Baksmaty, S. Yi, and N. P. Bigelow, *Phys. Rev. Lett.* **94**, 190401 (2005); K. Kasamatsu and M. Tsubota, *ibid.* **97**, 240404 (2006).
 - [15] E. A. Ostrovskaya and Y. S. Kivshar, *Phys. Rev. Lett.* **93**, 160405 (2004); T. J. Alexander, E. A. Ostrovskaya, A. A. Sukhorukov, and Y. S. Kivshar, *Phys. Rev. A* **72**, 043603 (2005).
 - [16] B. B. Baizakov, B. A. Malomed, and M. Salerno, *Europhys. Lett.* **63**, 642 (2003); *Phys. Rev. E* **74**, 066615 (2006).
 - [17] E. Poli, T. Bland, S. J. M. White, M. J. Mark, F. Ferlaino, S. Trabucco, and M. Mannarelli, *Phys. Rev. Lett.* **131**, 223401 (2023).
 - [18] A. Gallemí, S. M. Roccuzzo, S. Stringari, and A. Recati, *Phys. Rev. A* **102**, 023322 (2020).
 - [19] A. Gallemí and L. Santos, *Phys. Rev. A* **106**, 063301 (2022).

- [20] E. Casotti, E. Poli, L. Klaus *et al.*, [arXiv:2403.18510](https://arxiv.org/abs/2403.18510).
- [21] F. Ancilotto, M. Barranco, M. Pi, and L. Reatto, *Phys. Rev. A* **103**, 033314 (2021).
- [22] J. W. Reijnders and R. A. Duine, *Phys. Rev. Lett.* **93**, 060401 (2004); S. Tung, V. Schweikhard, and E. A. Cornell, *ibid.* **97**, 240402 (2006).
- [23] A. Marte, T. Volz, J. Schuster, S. Durr, G. Rempe, E. G. M. van Kempen, and B. J. Verhaar, *Phys. Rev. Lett.* **89**, 283202 (2002).
- [24] A. Ralston and H. S. Wilf, *Mathematical Methods for Digital Computers* (Wiley, New York, 1960).
- [25] Y. Pomeau and S. Rica, *Phys. Rev. Lett.* **72**, 2426 (1994); N. Sepulveda, C. Josserand, and S. Rica, *Eur. Phys. J. B* **78**, 439 (2010).
- [26] M. Pi, R. Mayol, A. Hernando, M. Barranco, and F. Ancilotto, *J. Chem. Phys.* **126**, 244502 (2007).
- [27] M. Sadd, G. V. Chester, and L. Reatto, *Phys. Rev. Lett.* **79**, 2490 (1997).
- [28] F. Ancilotto, M. Barranco, and M. Pi, *Phys. Rev. B* **97**, 184515 (2018).
- [29] C. A. Jones and P. H. Roberts, *J. Phys. A: Math. Gen.* **15**, 2599 (1982); A. Griffin, V. Shukla, M.-E. Brachet, and S. Nazarenko, *Phys. Rev. A* **101**, 053601 (2020).
- [30] A. Richaud, V. Penna, and A. L. Fetter, *Phys. Rev. A* **103**, 023311 (2021).
- [31] A. Bellettini, A. Richaud, and V. Penna, *Phys. Rev. A* **109**, 053301 (2024).
- [32] A. J. Groszek, D. M. Paganin, K. Helmerson, and T. P. Simula, *Phys. Rev. A* **97**, 023617 (2018).
- [33] F. Ancilotto (unpublished).
- [34] M. Tsubota, K. Fujimoto, and S. Yui, *J. Low Temp. Phys.* **188**, 119 (2017).
- [35] C. Nore, M. Abid, and M. E. Brachet, *Phys. Fluids* **9**, 2644 (1997).
- [36] A. S. Bradley and B. P. Anderson, *Phys. Rev. X* **2**, 041001 (2012).
- [37] See Supplemental Material at <http://link.aps.org/supplemental/10.1103/PhysRevA.110.013302> for some additional results on vortex dipole real-time dynamics in 2D triangular and honeycomb lattices.
- [38] M. Greiner, M. O. Mandel, T. Esslinger, T. Hansch, and I. Bloch, *Nature (London)* **415**, 39 (2002).
- [39] B. T. E. Ripley, D. Baillie, and P. B. Blakie, *Phys. Rev. A* **108**, 053321 (2023).